Journal of Environmental Management 246 (2019) 345–354

Contents lists available at ScienceDirect

Journal of Environmental Management

journal homepage: www.elsevier.com/locate/jenvman

Research article

Evaluation of pyrolyzed areca husk as a potential adsorbent for the removal of Fe^{2+} ions from aqueous solutions

B. Sheeka Subramani*, S. Shrihari, B. Manu, K.S. Babunarayan

Department of Civil Engineering, National Institute of Technology Karnataka, Surathkal, 575025, India

ARTICLE INFO

Keywords:
Pyrolysis
Areca husk
Iron removal
Adsorption Isotherms & Kinetics
Adsorption mechanism

ABSTRACT

The hurdle of valorisation of Arecanut husk on one side and the pollution of aquatic bodies by heavy metals like Iron on the other end are contemplated together in this study. The areca husk is pyrolyzed at 450°C for two hours to obtain Biochar. Batch adsorption studies were employed to investigate the effect of adsorbent dosage (2-10 g/l), initial concentration of adsorbate (1-5 mg/l) and contact time (30 -360 min) at temperature of 28 ± 2 °C & pH 4.0 ± 0.2 on the removal of Iron from pyrolyzed areca husk. The adsorption capacity was found to increase with increase in initial Iron concentartion and contact time, but decreases with the adsorbent dosage. Langmuir, Freundlich, Temkin and Dubinin-Radushkevich Isotherms was used to analyse the equilibrium data. Langmuir and Dubinin-Radushkevich model best describe the uptake of Iron ions implying a monolayer adsorption with physisorption. Pseudo second order, exhibited the best fit for the effectiveness of Iron adsorbtion indicating the maximum limit of chemisorption. Thermodynamic studies indicated that the adsorption was spontaneous and exothermic in nature. The mechanisms responsible for adsorption of Iron on pyrolysed areca husk was conducted by SEM-EDAX, XRD and FTIR indicating oxidation and precipitaion of Iron into complex compounds of jarosite and ferrous hydroxy sulphates. In conclusion, pyrolyzed areca husk can be technically & economically feasible alternative adsorbent material.

1. Introduction

Heavy metal induced aquatic contamination is one of the most serious environmental problems. It has gained relatively more significance in view of their persistence, bio-magnification and toxicity. Their presence in the ecosystem poses human health risks and causes harmful effects to organisms living in it and ones consuming them (Kadirvelu et al., 2002).

Iron is the most common element found in the earth's crust. Surface and Rain Water, trickling down through rock and soil can dissolve Iron, which reacts with oxygen resulting in formation of insoluble compounds, which then precipitates downwards to contaminate the ground water aquifers. Iron having divalent ions (Fe^{2+}) in water, is considered as a contaminant because of its organoleptic properties. Worldbank.org states that India is the largest consumer of ground water in the world. Over 85% of drinking water sources & 60% of irrigated agriculture are dependent on ground water (Ellis et al., 2000).

Iron in ground water can turn insoluble when exposed to air, giving it a brown red color. These problems could be of aesthetic nature, or causing indirect health concerns and in-turn economic problems (Jusoh et al., 2005). Altered taste can be noted at Iron concentrations above 40 μg/l. In well water, Iron concentrations up to 0.3 mg/l were notified as permissible. Rust colored silt seen in ground water is often an insoluble precipitate of Iron Hydroxide. Iron pipes could corrode and source Iron into the water transmitting through them. Water containing the above element may have altered taste, odor, color and turbidity. Above which, staining of laundry & plumbing issues may occur. A commonly noted slimy coating on the piping's of water distribution systems is actually an undesirable bacterial growth promoted by the Iron contents (Goher et al., 2015).

Various methods have been suggested to remove metals from water and wastewater, such as chemical precipitation, ion exchange, cementation, coagulation and flocculation, complexation, biosorption, adsorption, and membrane processes. However, most of these processes are expensive with high chemical and energy input (Kadirvelu et al., 2001). Among these techniques, adsorption seems to be an ideal process. These adsorbents can be assumed to be low cost since they can be prepared easily from agricultural waste and require less processing (De Gisi et al., 2016). Activated carbon has the strongest physical adsorption forces or the highest volume of adsorbing porosity of any known material. It is highly porous therefore it has an extremely high surface area for contaminant adsorption (Duman et al., 2009); (Ekpete and

* Corresponding author.
E-mail address: sheekasubramani5@gmail.com (B. Sheeka Subramani).

https://doi.org/10.1016/j.jenvman.2019.04.122
Received 12 February 2019; Received in revised form 25 April 2019; Accepted 29 April 2019
Available online 08 June 2019

Horsfall, 2011). Activated carbon can be characterised by a large specific surface area up to 500–2500 m^2/g and this forms the dominant property that allows adsorption. Activated carbon removes heavy metals by complexation and by electrostatic attraction of metal ions to various surface oxygen-containing surface groups.

Many researchers have been investigating low-cost adsorbents for heavy metal removal such as sawdust, rice husk, sago waste, red pepper seeds, barks, teak leaves powder, saltbush leaves, palm kernel fibre, groundnut shells, tree fern, chitosan, etc. (Kadirvelu et al., 2003). Areca husk is a solid waste largely generated from plantations and left unutilized on the fields, causing a significant disposal problem. Wide expanse of cultivation of Areca catechu (Arecaceae) is observed mainly in Southeast Asia and other parts of Southern Asia. In India, Arecanut production crossed 7.3 lakh tonnes during 2015–16 (http://www.dasd.gov.in/). Owing to increased reports of health hazards due to Arecanut use and growing outcry to ban arecanut in the chewing form has inspired Researchers and Progressive growers to find alternative uses for arecanut. The fibrous outer cover of the betel nut which accounts to a large portion of the volume & weight of the fruit, called the husk, has found some use as raw material for hardboards & packaging material. However, in most cases, the growers consider it a waste byproduct & use it as an inferior fuel and mulch (Peng et al., 2015). Instead of this, Areca husk can be pyrolyzed into biochar and used as an adsorbent for the removal of heavy metals like Iron from contaminated water, minimizing waste accumulation. In this regard, this study is innovative in testing the efficacy of activated carbon derived from areca husk as a potential adsorbent to treat water to permissible limits.

2. Materials and methods

2.1. Chemicals and reagents

The adsorbate Ferrous Sulfate Heptahydrate ($Fe_2SO_4.7H_2O$) was purchased from Merck. The stock solution of 1000 mg/l was prepared with 4.978 g of $Fe_2SO_4.7H_2O$ in 1000 ml deionised water. Concentration of Iron was measured using UV-VIS Double Beam Spectrophotometer (Systronics Make, AU-2701 Model) at 510 nm 1,10 Phenanthroline method was used to determine the concentration which reacts with ferrous ions forming reddish orange color(Harvey et al., 1955).

2.2. Preparation of areca husk adsorbent

The arecanut husk is obtained from an areca plantation in Thirthalli town of Karnataka. The husk is washed repeatedly for removal of dirt and other impurities with water & deionised water before oven drying. The husk rendered ready was oven dried at 378 K (105 °C) for 24 h until the residual moisture was completely evaporated.

Results of proximate analysis of the husk adsorbate carried out as per ASTM standards are presented in Table 1. It is seen that the high fixed carbon and low ash content justify suitability of arecanut husk as an activated carbon precursor.

Pyrolysis of arecanut husk was carried out in a muffle furnace at 450 °C for 2 h. The pyrolyzed sample was then ground with the help of ball mill to obtain particle size range to 40–80 mesh. The ground pyrolyzed areca husk was suspended and agitated for 2 h on ultrasound bath. The suspension was filtered and dried in the oven (Indhumathi et al., 2014). The resulting sample was carefully stored in desiccators for characterization and adsorption experiments.

Table 1
Proximate analysis of arecanut husk.

Parameter	Weight % (on dry basis)
Moisture	8.23
Volatile matter	57.01
Ash	3.16
Fixed carbon	31.6

2.3. Characterization of adsorbent

The surface morphology of pyrolyzed areca husk was examined using scanning electron microscopy (SEM) attached with energy dispersive X-ray (EDAX) analyzer (Zeiss EVO MA18 with Oxford EDS (X-act)). The surface area, total pore volume, and pore size distribution of all samples were determined by N_2 adsorption at −196 °C using Autosorb (Quantachrome Corp.). The surface area and pore volume were obtained by applying the Brunauer-Emmett-Teller (BET) equation to the adsorption data.

X-ray diffraction (XRD) patterns of pyrolyzed areca husk is obtained with an automated Rigaku 600 instrument using Cu Kα radiation at 40 kV and 30 mA over the range (2θ) of 10°–90°, with a scanning speed at 2° per minute. Fourier transfer infrared (FT-IR) spectra were collected on a Shimadzu with a resolution of 4 cm^{-1} by using the KBr technique. The spectrum was scanned from (400–4000 cm^{-1}). The pH_{zpc} of pyrolyzed areca husk was experimentally found by pH drift method.

2.4. Adsorption experiments

Data Acquisition - Different amounts of pyrolyzed areca husk (2, 4, 6, 8 and 10 g) were added into 300-ml stoppered glass bottles containing a fixed volume (100 ml in each flask) of varied initial concentration (1, 2, 3, 4 and 5 mg/l) of synthetic Iron solution at pH between 4.0 ± 0.2, at an ambient temperature of 28 ± 2 °C. The bottles were placed in a shaker (Rotek, India) and agitation was provided at 150 rpm for 6 h and the Iron concentrations were measured at 1 h interval.

Data Analysis – From the experimental data, adsorbent performing characteristics were obtained. Concentration reduction of Iron at various time intervals were computed and from plots of adsorption amount versus contact time for various adsorbent dosages for different initial concentrations were understood and appraised. All experiments were conducted in duplicate to minimise any errors.

Available popular and recognised Isotherm models like Langmuir, Freundlich, Temkin and the Dubinin-Radushkevich (D-R) (Goher et al., 2015); (Hameed, 2009); (Girods et al., 2009) were considered to describe how adsorbents interact with solutes. The linearized forms of the four isotherms are

$$\frac{1}{q_e} = \frac{1}{q_m} + \frac{1}{(k_l q_m)} \frac{1}{C_e} \quad (1)$$

$$\ln q_e = \ln K_f + \frac{1}{n} \ln C_e \quad (2)$$

$$q_e = B \ln A + B \ln C_e \quad (3)$$

$$\ln qe = Xm - \beta\varepsilon^2 \quad (4)$$

The Langmuir constants q_m (mg/g) and k_1 (l/mg) are related to adsorption capacity and energy of adsorption, respectively. The constants q_m and k_1 can be determined from the plot $1/q_e$ versus $1/C_e$ (Eq. (1)). C_e (mg/l) and q_e (mg/g) are the equilibrium concentration and the amount of Iron adsorbed at equilibrium, respectively. Similarly, the Freundlich Isotherm constants K_f and 1/n can be calculated from the plot of $\ln(q_e)$ versus $\ln(C_e)$ (Eq. (2)). K_f and n are the Freundlich constants, which are indicators of adsorption capacity and adsorption intensity, respectively. The Temkin isotherm has generally been applied in the form given by Eq. (3). Therefore, plotting q_e versus $\ln C_e$, enables the determination of the constants A and B. B is the Temkin constant related to heat of sorption (J/mol), A is the Temkin isotherm constant (l/g). The Dubinin-Radushkevich (D-R) equation sheds detail on the

type of adsorption as in whether it is physisorption or chemisorption. ε (Polanyi potential) = RT ln(1 + 1/C_e), X_m = ln q_m, q_m is the maximum adsorption capacity (mg/g), β is related to mean free energy, E (E in kJ/mol) as:

$$E = \frac{1}{\sqrt{-2\beta}}$$

The most common models used to fit the kinetic sorption experiments were Lagergren's pseudo-first-order model (Eq. (5)) and pseudo-second-order model (Eq. (5)): (Liang et al., 2010)

$$\log(q_e - q_t) = \log q_e - \frac{K_1\, t}{2.303} \quad (5)$$

$$\frac{t}{q_t} = \frac{1}{K_s q_e^2} + \frac{1}{q_e}\, t \quad (6)$$

where q_e (mg/g) and q_t (mg/g) are the amount of adsorbate adsorbed at equilibrium and at time t, respectively. K_1 (min^{-1}) and K_s (g mg^{-1} min) are the pseudo-first-order and pseudo-second order adsorption rate constants, respectively.

2.5. Intraparticle diffusion model

To investigate the mechanism of Iron adsorption onto pyrolyzed areca husk, intraparticle diffusion-based mechanism was studied. The most commonly used technique for identifying the mechanism involved in the adsorption process is by fitting an intra particle diffusion plot. It is an empirically formulated functional relationship, familiar to most adsorption processes, where the uptake varies almost proportionally with $t^{1/2}$. According to the theory proposed by Weber and Morris

$$q_t = k_{id} t^{1/2} + C_i \quad (7)$$

where k_{id} (mg g^{-1} $min^{1/2}$), the rate parameter of stage i, is obtained from the slope of the straight line of q_t versus $t^{1/2}$. C is the intercept (Wu et al., 2009).

3. Results and discussion

The results of the current investigation are presented and discussed in the section that follows.

3.1. Characterisation of adsorbent

The SEM image detected the structure of the pyrolyzed areca husk as porous and amorphous which is supported by XRD results (see Fig. 1). The areca husk is mainly composed of lignin and cellulose composites bonded together which degraded to create much corrugated sheet like structure creating active adsorption sites (Supriadi et al., 2017). EDAX measurement was carried to ascertain the elemental composition in the prepared pyrolyzed areca husk. The raw areca husk had 31.6% fixed carbon which enriched to more than 75% after the pyrolysis process as observed from EDX result and this may be attributed to areca husk not being volatilized and the higher level of carbon content in the areca husk feedstock.

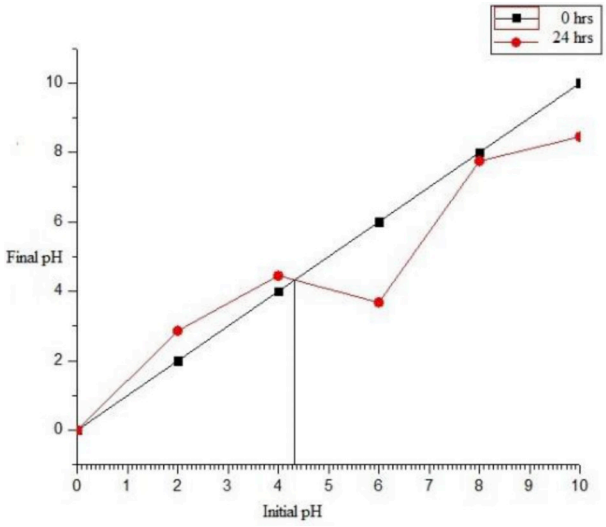

Fig. 2. phzpc of pyrolyzed areca husk.

The XRD result consisted of distinct, broad peaks ranging from 2θ ~20°–28°, and a weak peak at ~43°. These peaks are assigned as (002) and (001) graphite planes, respectively. The broad initial peaks at (002) graphite plane were centred at ~ 25° which is attributed to the lower reflection then graphite at around 27°, thus displaying a significant level of interlayer d spacing (3.67 Å) which was similar to the observations of coir-pith by Supriadi et al. (2017).

The peaks obtained in the FTIR spectrum decide the participation of surface functional groups in adsorption interaction. The IR spectra exhibited broad peaks at 3382 cm^{-1} indicating O–H stretching vibration of hydroxyl functional groups. The presence of peaks at 2920 cm^{-1} and 2851 cm^{-1} is related to methyl C–H stretching. At 2360 cm^{-1} peak, C═O stretching was indicated. The band at 1590 cm^{-1} is attributed to the presence of highly conjugated C–O in carbonyl structure. The overlapping bands at 400 cm^{-1} to 500 cm^{-1} is due to the stretching vibration of S–S of Polysulphides and Aryl disulphides. (Kavitha and Namasivayam, 2008). The results from FTIR analysis indicate that the surface contains acidic functional groups, which increases metal ion adsorption.

The surface area, using N_2 as adsorbate at 196 °C measured the

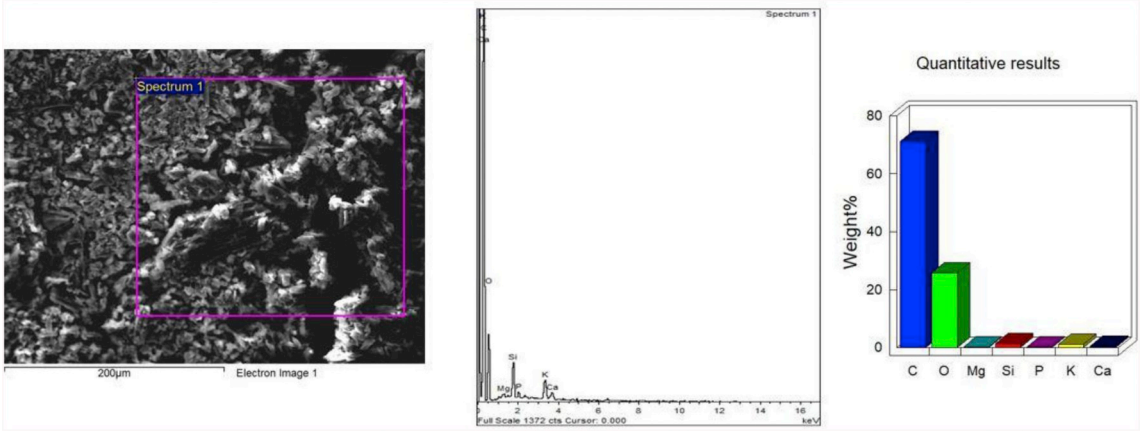

Fig. 1. SEM of pyrolyzed areca husk.

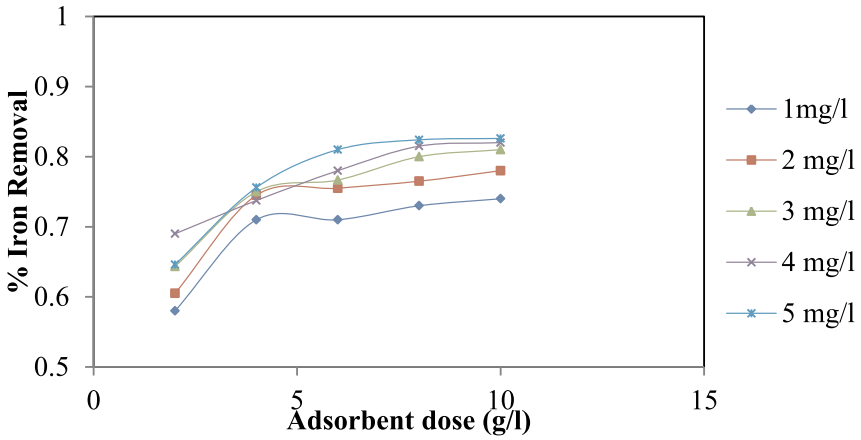

Fig. 3. Effect of adsorbent dosage on the adsorption of Iron on pyrolyzed areca husk (Time = 5 h and Co = 1, 2, 3, 4 & 5 mg/l).

specific surface area as 54.5 m^2/g and the volume of the pore as 0.0142 cm^3/g. The surface charge of the biochar in the aqueous media conducted experimentally by a pH drift method (see Fig. 2) to finalize the optimum phzpc or ph point of zero charge of the adsorbent material. The point of zero charge (pHzpc) on pyrolyzed areca husk is 4.2 $meq{\cdot}g^{-1}$ indicating acidic functional groups which are confirmed by the FTIR results. This suggests that the pyrolyzed areca husk surface releases hydroxide groups into the solution, hence the adsorbent surface is positively charged attracting anions (Rahman et al., 2014).

The newly produced carbonized areca husk is cost effective and is estimated at around 1.4 USD/kg. From the internet search results, the cost of commercially available activated charcoal varies from USD 2.2 to 5 (Selvaraju and Bakar, 2017). Hence, this carbonized areca husk can be used as an alternative which is more promising and a cleaner adsorbent. The rates were estimated based on the price rate in India. The details are given in supplementary table 1 (Liew et al., 2019).

3.2. Performance appraisal of pyrolyzed arecanut husk for iron removal

The experimental setup and methodology for the parametric studies made in this investigation is elaborated in the sections that follow.

3.2.1. Effect of adsorbent dose on iron adsorption

The maximum removal efficiency of about 80% Iron is obtained at 10 g/l of pyrolyzed arecanut husk dosage. As seen from Fig. (3), the increase in adsorbent quantity (w = 2, 4, 6, 8 & 10 g/l) for the same initial Iron concentration (1–5 mg/l), the amount of Iron adsorbed by pyrolyzed arecanut husk for Iron removal reduced gradually. This is attributed to the aggregation of adsorbent at a higher dosage and subsequent reduction of adsorption sites. A similar response is reported in the experimental investigation for the adsorption of Iron on commercially available granular activated carbon by Jusoh et al. (2005)

3.2.2. Effect of initial concentration and contact time

Fig. 4 shows the effect of initial concentration (1–5 mg/l) on adsorption of Iron on pyrolyzed arecanut husk at 28 ± 2 °C. It is observed that the gradient of q_t versus contact time is steep for the first 30–60 min and then the gradient flattens. The rapid adsorption in the initial stage is due to the availability of a large number of adsorption sites. The adsorption capacity of pyrolyzed Arecanut husk (w = 2 g/l) for Iron removal by batch process increased from 0.05 to 1.8 mg/g with a high initial concentration of Iron.

3.3. Adsorption isotherms

Adsorbent Isotherms are important in understanding the performance of solutes. They are mathematical models that describe the behavior between solid and liquid phases for the adsorbate species. The equilibrium between the amount of contaminant adsorbed by carbonized arecanut husk and the concentration of the dissolved contaminant Iron is given by adsorption Isotherm. Langmuir, Freundlich, Temkin, and Dubinin-Radushkevich isotherm model is the most often used isotherms to describe the adsorption data for contaminant concentration.

According to Langmuir adsorption isotherm, there is only monolayer adsorption on the adsorbent. The equilibrium distribution of the contaminant Iron between the solid and liquid phases is given by a single layer. There is no adsorption occurring after this monolayer is formed atop the adsorbent. This kind of single layer adsorption takes place on the adsorbent surface which has a restricted number of similar sites. This model used in bio-sorption processes is given by the equation:

$$q_e = \frac{q_m C_e}{1 + k_l C_e} \tag{8}$$

The linearized form of the isotherm is

$$\frac{1}{q_e} = \frac{1}{q_m} + \frac{1}{(k_l q_m)} \frac{1}{C_e} \tag{9}$$

where, C_e – equilibrium Iron ion concentration (mg/l) & q_e – amount of Iron adsorbed at equilibrium (mg/g). k_l (l/mg) and q_m (mg/g) are Langmuir constants related to energy of adsorption and adsorption capacity respectively.

The Freundlich isotherm model is based on the heterogeneous distribution of active sites accompanied by interactions between molecules adsorbed. The following equation expresses this model:

$$q_e = C_e^{1/n} k_f \tag{10}$$

The linearized form of the isotherm is

$$\ln q_e = \ln k_f + \frac{1}{n} \ln C_e \tag{11}$$

where, k_f (mg/g) and 1/n are Freundlich constants related to relative adsorption capacity of carbonized arecanut husk and intensity of adsorption & indicate the tendency of the adsorbate to be adsorbed.

The Temkin isotherm assumes the heat of adsorption increases linearly with decreasing coverage. The following equation expresses this model:

$$Q_e = B \ln A + B \ln C_e \tag{12}$$

where, B = RT/b, is the Temkin constant related to heat of sorption (J/mol), A is the Temkin isotherm constant (l/g), R is the gas constant (8.314 J/mol K), b is Temkin isotherm constant, and T is the absolute temperature (K).

The Dubinin-Radushkevich (D-R) equation sheds detail on the type of adsorption as in whether it is physisorption or chemisorption and

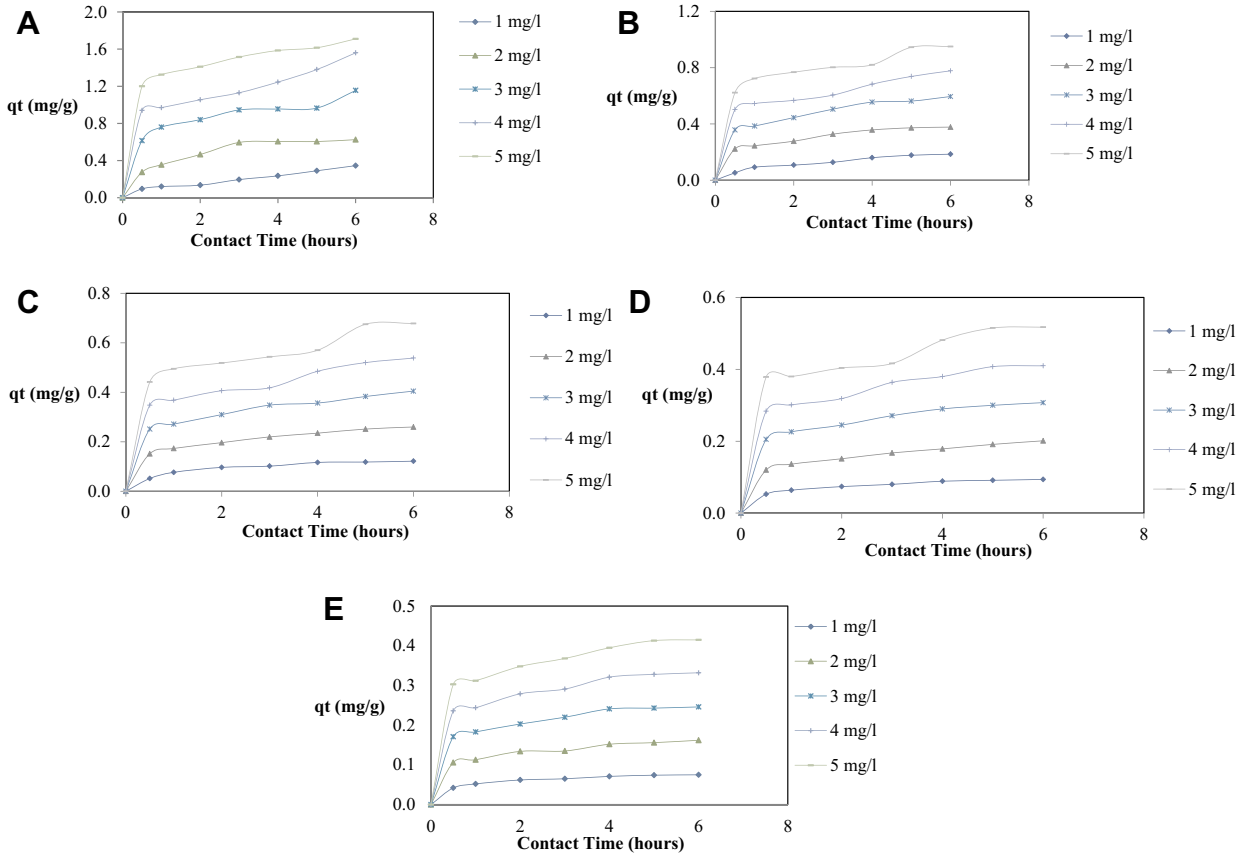

Fig. 4. (a–e): Effect of initial concentration and contact time on Fe adsorption (W = 2,4,6,8 & 10 g; V = 1 l).

expressed as

$$\ln qe = Xm - \beta\varepsilon^2 \quad (13)$$

where ε (Polanyi potential) = RT ln(1 + 1/C_e), X_m = ln q_m, q_m is the maximum adsorption capacity (mg/g), β is related to mean free energy, E (E in kJ/mol) as:

$$E = \frac{1}{\sqrt{-2\beta}} \quad (14)$$

Table 2 shows that Langmuir, Freundlich, Temkin and D-R isotherm model fitted well for Iron ions on Pyrolyzed areca husk with a high coefficient of correlation (R^2) values. Langmuir adsorption isotherm presented a better fit for the experimental data. The value of k_l indicated the affinity of Iron ions with pyrolyzed areca husk. The maximum adsorption potential of pyrolyzed areca husk for Iron removal was 0.379 mg/g by Langmuir isotherm which was in accordance with the obtained experimental data [Fig. 5]. The R_L value indicated that the adsorption of Iron by pyrolyzed areca husk as a favorable process.

Even though the coefficient of co-relation (R^2) was high for Freundlich isotherm, the value of n was lesser than 1 which states an unfavorable tendency for the adsorbate to adsorb. This is attributed to the decrease in adsorption sites due to saturation. The correlation coefficient for Temkin Isotherm model is 0.838 indicating average linearity. The mean free energy, E calculated from D-R isotherm study is 1.55 kJ/mol which is less then 8 kJ/mol suggesting that adsorption follows physisorption (Kundu and Gupta, 2006).

From the results, it is evident that Langmuir and D-R isotherm model is the best predictor of the process of adsorption of Iron on Pyrolyzed Areca husk and also suggest carbonized areca offers monolayer adsorption surface and follows physisorption mechanism.

3.4. Adsorption kinetics

Adsorption kinetics are essential tools for evaluating the effectiveness of adsorption. Lagergren's pseudo-first-order and pseudo-second-order models have been employed to clarify adsorption Kinetics of Iron ions onto pyrolyzed areca husk. For Kinetic studies, different concentrations of Iron ranging from 1 to 5 mg/l and contact time of 0.5, 1, 2, 3, 4, 5 and 6 h is used at an optimum bio-sorbent concentration of 10 mg/l.

The Lagergren model is a pseudo-first-order rate equation and is as follows:

$$\log(q_e - q_t) = \log q_e - \frac{k_l\, t}{2.303} \quad (15)$$

where, q_e and q_t are the amounts of adsorbed metal ion (mg/g) at equilibrium and at time t (hours), respectively. k_1 is the Lagergren rate constant relating to adsorption energy (l/min).

Table 2
Langmuir, Freundlich, Temkin and Dubinin-Radushkevich isotherm parameters.

Langmuir isotherm				Freundlich isotherm			Temkin isotherm			Dubinin- Radushkevich isotherm			
k_l	q_{max}	R^2	R_L	n	k_f	R^2	A	B	R^2	Xm	β	E	R^2
1.579	0.379	0.993	0.136	0.367	0.713	0.954	1.525	1.926	0.838	0.65	0.208	1.55	0.99

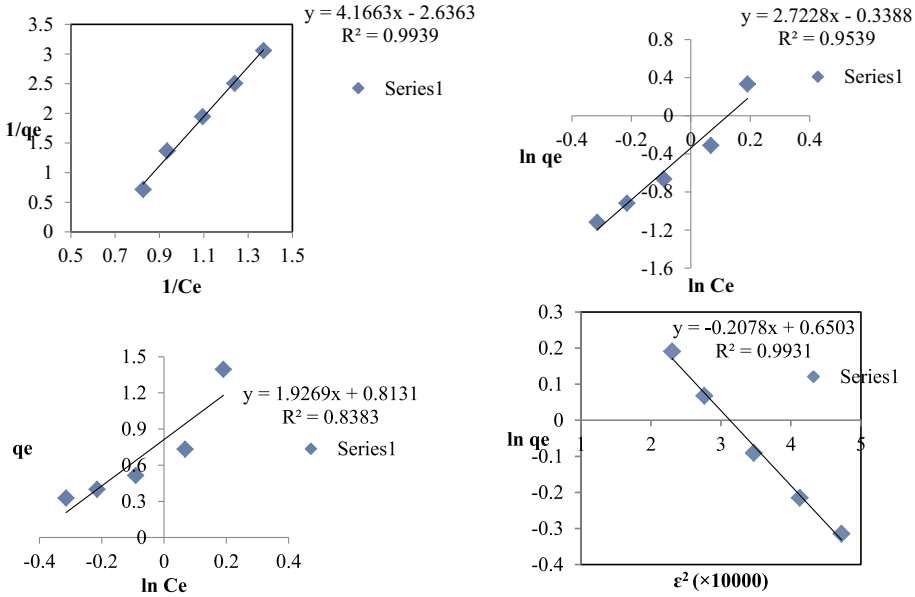

Fig. 5. Plots for Langmiur (a), Freundlich (b), Temkin (c) and Dubinin-Radushkevich (d) isotherms for Iron on pyrolyzed arecanut husk (C_o = 4 mg/l, Adsorbent = 2,4,6,8 & 10 mg/l).

Table 3
Lagergren's first-order and Pseudo-second-order kinetic parameters for the adsorption of Iron on Carbonized areca husk.

Initial concentration (mg/l)	q_e (exp) (mg/g)	Pseudo-first-order kinetics			Pseudo-second-order kinetics		
		k_1 (min^{-1})	q_e (cal) (mg/g)	R^2	q_e (cal) (mg/g)	k_s (g/mg^{-1} hour)	R^2
1	0.073	0.65	0.041	0.88	0.081	20.84	0.99
2	0.157	0.63	0.075	0.70	0.171	11.25	0.99
3	0.243	0.87	0.145	0.77	0.262	8.89	0.99
4	0.327	0.74	0.166	0.79	0.352	6.65	0.99
5	0.407	0.58	0.163	0.93	0.438	5.64	0.99

The values of k_1 and q_e is presented in Table 3.

The pseudo-second-order kinetic model of McKay and Ho is expressed as follows:

$$\frac{t}{q_t} = \frac{1}{k_s q_e^2} + \frac{1}{q_e} t \quad (16)$$

where, q_e and q_t are the amounts of Iron adsorbed (mg/g) at equilibrium and at time t (hours), respectively. k_s (g/mg/hour) is the rate constant of pseudo-second-order kinetics.

The values of q_e and k_s that is presented in Table 3 are calculated from the slope and intercept of t/q_t versus t (see Fig. 6).

From Table 3, it is evident that q_e values obtained from the pseudo-second-order kinetic model are in close agreement with experimental and best described the behavior of Iron adsorption onto Pyrolyzed areca husk.

The mechanism of the Iron adsorption onto pyrolyzed areca husk is studied by intra-particle diffusion also. According to the theory proposed by Weber and Morris:

$$q_t = k_{id} t^{1/2} + C_i \quad (17)$$

where, k_{id} (mg g^{-1} $min^{1/2}$), the rate parameter at stage i, is obtained from the slope of the straight line of q_t versus $t^{1/2}$.

The kinetic results is analyzed by using the intra-particle diffusion model. Weber and Moris plot (q_t versus $t^{0.5}$) were used to inspect the intra-particle diffusion mechanism. (Table 4). The rate of adsorption is controlled by intra-particle diffusion for the entire adsorption period, if the value of C_i is zero. However, the plot of q_t against $t_{0.5}$ usually shows more than one linear portion. As seen from Fig. 7., the plots were non-linear over the whole-time range, implying that the adsorption was affected by more than one process.

3.5. Desorption studies

It is essential to know the desorption behavior of Iron from carbonized areca husk to get an overall understanding of the adsorption mechanism. Carbonized areca husk can be used multiple times only if it can be regenerated using a suitable eluent. In the present study 0.1 M HCl, HNO_3, H_2SO_4 is explored for Iron desorption capability from Carbonized areca husk.

From Fig. 8, it is understood that 95% of the adsorbed ferrous ions is desorbed from carbonized areca husk with 0.1 M HNO_3 giving optimum results. The acid environment lets the protonation on the surface of carbonized areca husk which allows the desorption of ferrous ions easily (Kołodyńska et al., 2017). Acid containing waters precipitate a plethora of minerals on the carbonized areca husk. At lower pH, jarosite or amorphous ferric hydroxy sulphates may form. Formation of the well-crystalline ferric sulfate minerals may require prolonged time. The ferric compounds form a wide variety of complex metal precipitates (Majzlan and Myneni, 2005). The contribution of ferrous salt precipitation with minerals can be explained with the quantitative analysis by XRD.

The adsorption-desorption cycle of ferrous ions on carbonized areca husk was repeated two times to check its reusability. There was no significant change in the adsorption potential of Carbonized areca husk during its operation, rendering it possible for repeated use.

3.6. Adsorption mechanism for the adsorption of iron on carbonized areca husk

3.6.1. Thermodynamic studies

To investigate the adsorption feasibility of Iron on carbonized areca husk, thermodynamic studies are carried out at different temperatures ranging from 313 K to 333 K for the different initial Iron concentration of 2, 3 and 5 mg/l. From the plot of ln Kc versus 1/T, it is found that the adsorption capacity decreased with an increase in temperature. The calculated values of the thermodynamic parameters are given in

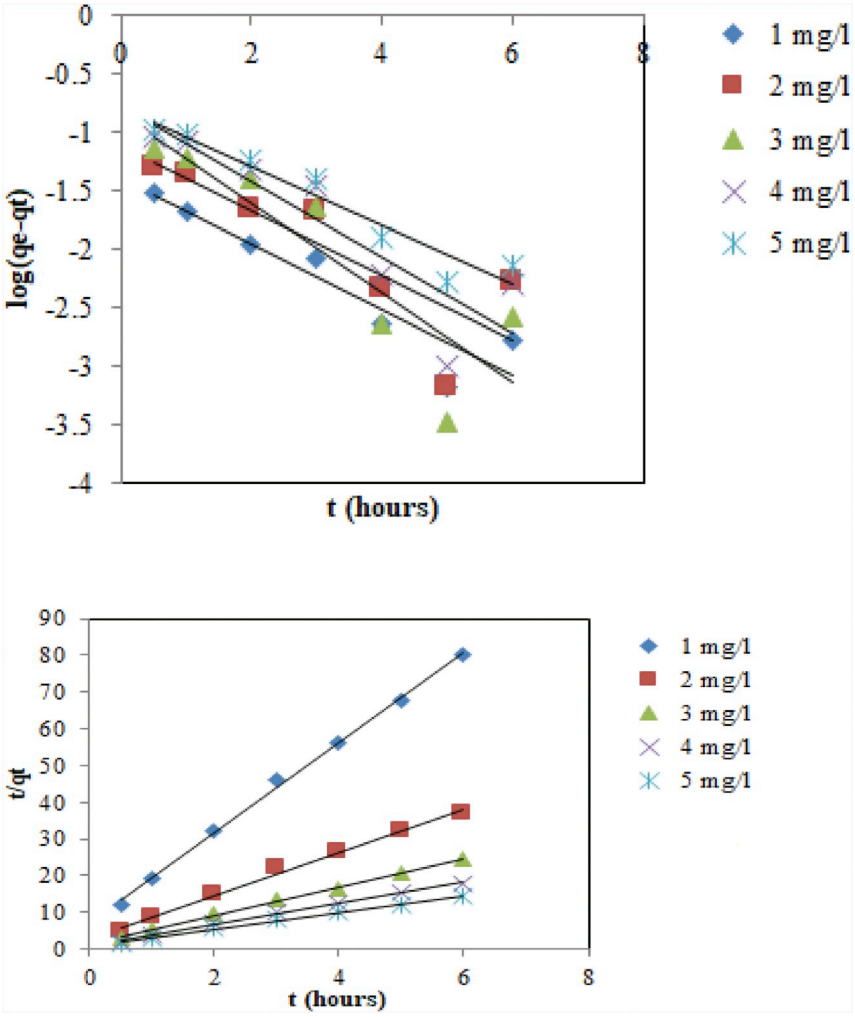

Fig. 6. Plots for Lagergren's pseudo-first-order and pseudo-second-order models for Iron on carbonized arecanut husk.

Table 4
Intra-particle diffusion model parameters for the adsorption of Iron on Carbonized areca husk.

Initial concentration (mg/l)	Intra-particle diffusion model		
	k_{id} (mg g^{-1} $min^{1/2}$)	C_i	R^2
1	0.043	0.27	0.96
2	0.037	0.23	0.94
3	0.028	0.17	0.93
4	0.020	0.10	0.94
5	0.011	0.04	0.88

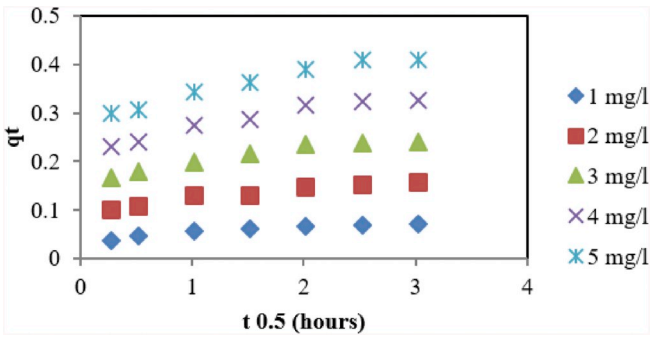

Fig. 7. Plot for intra-particle diffusion model for Iron on carbonized arecanut husk.

Table 5. The change in enthalpy (ΔH°) values found for the adsorption of Iron were negative due to the exothermic nature of the adsorption process. The negative values of ΔG° indicate that the adsorption process is spontaneous. Also, the negative values of ΔS° point out the associative mechanism involved during the process of adsorption, and there is a decrease in the randomness at the stable/solution interface during the adsorption process.

The initial concentration of the adsorbate was varied to investigate its effect on the thermodynamic parameters. Similar phenomena were seen for all the various initial concentration as shown in Fig. 9. The type of adsorption was investigated mainly using these parameters namely ΔH° - Enthalpy, ΔS - Entropy, E − Mean free energy and the effect of temperature. A negative value of ΔH° indicates that the adsorption of Iron on areca husk is exothermic that is, energy is liberated during the process. This usually occurs when adsorbate molecules are adsorbed on the surface, freedom of movement of molecules become restricted, and this results in a decrease in entropy. At constant temperature and pressure, adsorption occurs spontaneously. Gorzin and Bahri Rasht Abadi (2018) states that if the enthalpy change value is lower than 20 kJ/mol, then the process is physisorption indicating weak electrostatic bonding of metal ions on the adsorbent surface. From the study, we can observe that ΔH° and also ΔS° values are lower, and hence it follows physisorption.

3.6.2. Precipitation with minerals

Carbonized Areca husk was scanned by XRD (Fig. 10) after Iron adsorption to check its role in the precipitation of minerals. In contrast

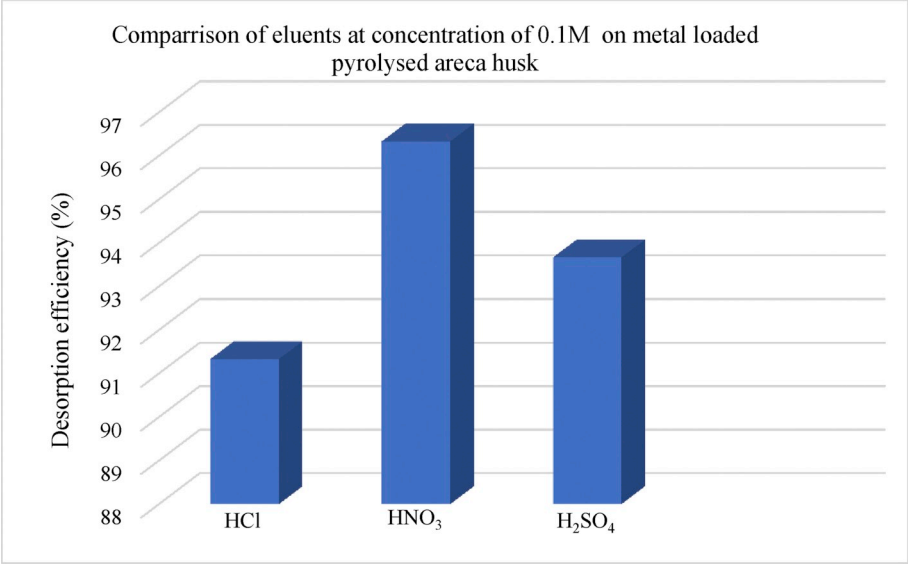

Fig. 8. Comparison of eluents at the concentration of 0.1 M on metal loaded pyrolyzed areca husk.

Table 5
Thermodynamic parameters for the adsorption of Iron on Carbonized areca husk.

T(K)	1/T (K)	Co (mg/l)	Ce (mg/l)	Cs = Co–Ce (mg/l)	Kc = Cs/Ce	ln Kc	ΔG°	ΔH°	ΔS°
303	0.0033	5	0.79	4.21	5.3291	1.673	−4.214	−6.953	−0.0091
313	0.0032	5	0.87	4.13	4.7471	1.557	−4.053		
323	0.0031	5	0.91	4.09	4.4945	1.502	−4.035		
303	0.0033	3	0.51	2.49	4.8823	1.585	−3.994	−7.275	−0.0108
313	0.0032	3	0.56	2.44	4.3571	1.471	−3.830		
323	0.0031	3	0.59	2.41	4.0847	1.407	−3.779		
303	0.0033	2	0.39	1.61	4.1282	1.417	−3.571	−11.946	−0.0278
313	0.0032	2	0.46	1.54	3.3478	1.208	−3.144		
323	0.0031	2	0.49	1.51	3.0816	1.125	−3.022		

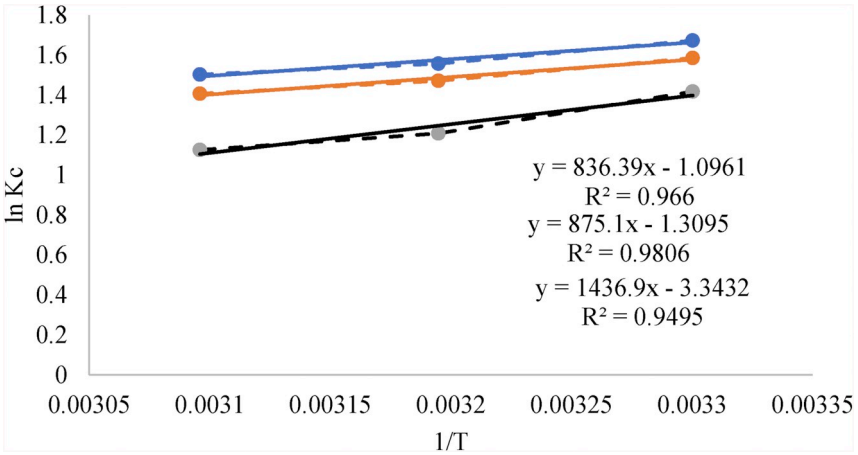

Fig. 9. Plot for ln Kc versus 1/T for the estimation of thermodynamic parameters for the adsorption of Iron on carbonized arecanut husk.

to original pyrolyzed areca husk, the results after adsorption of Iron showed significant changes. This may be attributed to the precipitation of Iron as Goethite (FeO(OH)), Limonite $FeO(OH)\cdot nH_2O$, Jarosite ($KFe_3^{3+}(OH)_6(SO_4)_2$), ferric hydroxy sulfates or both and probably metal phosphates or silicates and these results are partly supported by FTIR. The combined oxidation and precipitation of is described by the following equations.

The Fe^{2+} can oxidize into Fe^{3+}, which then hydrolyzes into "ferric hydroxides"

Oxidation reaction: $4Fe^{2+}(aq) + O_2 + 4H^+(aq) \leftrightarrow 4Fe^{3+}(aq) + 2H_2O$

Hydrolysis: $Fe^{3+}(aq) + 3H_2O \leftrightarrow Fe(OH)_3\ (s) + 3H^+$

(Hove et al., 2007).

Similarly, Oxidation of Iron led to the formation of Two types of ferric hydroxy sulfate precipitates from acid ferrous sulfate solutions. Jarosites were also precipitated by oxidation in $FeSO_4$ solutions containing suitable monovalent cations, such as Na^+, K^+ and an excess of sulfate anions at pH 2.5 (Lazaroff et al., 1982).

From SEM and EDS observations (Fig. 11), complexation of Fe^{2+}

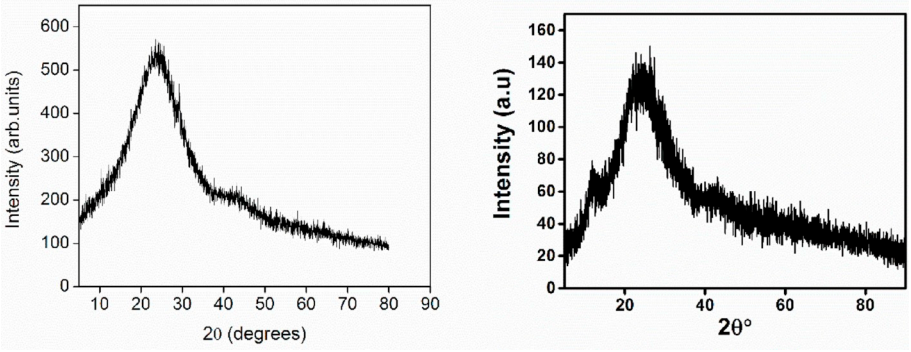

Fig. 10. XRD results of Pyrolyzed areca husk post adsorption of Fe^{2+}.

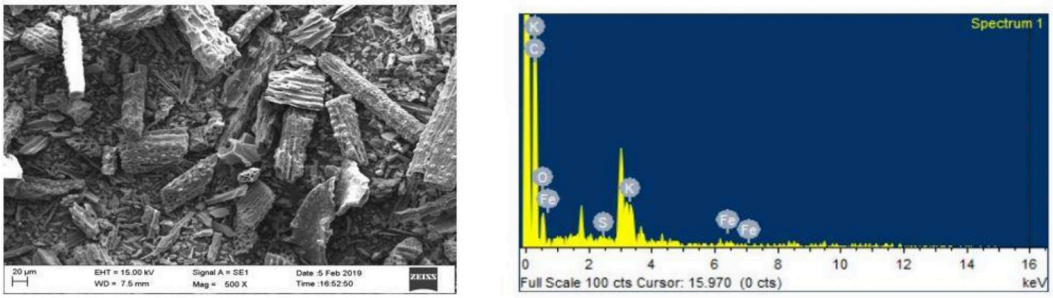

Fig. 11. SEM results of Pyrolyzed areca husk post adsorption of Fe^{2+}.

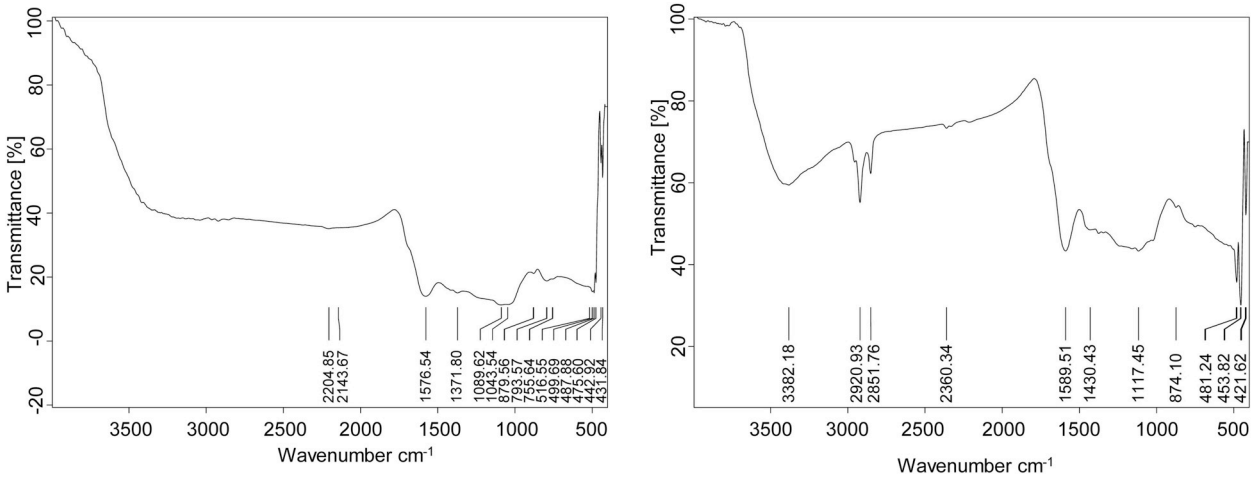

Fig. 12. FTIR results of Pyrolyzed areca husk befosre and after adsorption of Fe^{2+}.

ions have taken place on the surface with the Oxygen functional groups contributing to the adsorption capacity of pyrolyzed areca husk.

3.6.3. Complexation with functional groups

As shown in Fig. 12, the functional group at 3382 cm^{-1} representing the stretching vibration of the O–H group disappeared completely after interaction with the ferrous ions on the pyrolyzed areca husk. The bands at 2920 cm^{-1} and 2851 cm^{-1} corresponding to the Methyl C–H stretch also vanished indicating its participation in the process of adsorption. The bands at 1589 cm^{-1} assigned to Carboxylic acid salt weakened to C═O stretching vibrations of amides (1576 cm^{-1}). Sulfate ions are deformed by ferrous complexation or hydrogen bonding and are distinguished from hydrogen sulfate by the stretching bands at 880 cm^{-1}. Metal phosphates [$Fe_3(PO_4)_2$ & $FePO_4$] is precipitated at P–O stretching vibrations of PO_4^{3-} and was confirmed by the band at 1110 cm^{-1}. The typical bending, symmetric and asymmetric stretching of Si–O–Si were observed at 400 to 700 cm^{-1} which further confirmed the precipitation of Iron as FeO_4Si (Gao et al., 2019). On the whole, it suggested that the presence of many functional groups such as –OH, $–CH_3$ and –COOH are responsible for the adsorption of ferrous ions on pyrolyzed areca husk.

4. Conclusion

The utility of pyrolyzed arecanut husk as the adsorbent is experimentally investigated. Experimental results are compared and verified with available popular and recognised mathematical models. The study indicates that arecanut husk finds potential as an adsorbent with an indicated capacity of 0.38 mg/g for the kind of adsorbent developed and used in the study. Langmuir & D-R Isotherm and pseudo-second-order kinetics are best suited for the performance appraisal of pyrolyzed arecanut husk as an adsorbent. Thermodynamic studies indicated the process of adsorption as spontaneous and exothermic. Adsorption mechanism indicated oxidation and precipitation of Iron complexes along

with surface complexation with functional groups. Hence pyrolyzed arecanut husk can be a promising alternative to activated carbon for removal of Iron as it is more cost effective.

Appendix A. Supplementary data

Supplementary data to this article can be found online at https://doi.org/10.1016/j.jenvman.2019.04.122.

References

De Gisi, S., Lofrano, G., Grassi, M., Notarnicola, M., 2016. Characteristics and adsorption capacities of low-cost sorbents for wastewater treatment: a review. Sustain. Mater. Technol. 9, 10–40.

Duman, G., Onal, Y., Okutucu, C., Onenc, S., Yanik, J., 2009. Production of activated carbon from pine cone and evaluation of its physical, chemical, and adsorption properties. Energy Fuels 23 (4), 2197–2204.

Ekpete, O.A., Horsfall, M.J.N.R., 2011. Preparation and characterization of activated carbon derived from fluted pumpkin stem waste (Telfairia occidentalis Hook F). Res. J. Chem. Sci. 1 (3), 10–17.

Ellis, D., Bouchard, C., Lantagne, G., 2000. Removal of iron and manganese from groundwater by oxidation and microfiltration. Desalination 130 (3), 255–264.

Gao, L.Y., Deng, J.H., Huang, G.F., Li, K., Cai, K.Z., Liu, Y., Huang, F., 2019. Relative distribution of Cd2+ adsorption mechanisms on biochars derived from rice straw and sewage sludge. Bioresour. Technol. 272, 114–122.

Girods, P., Dufour, A., Fierro, V., Rogaume, Y., Rogaume, C., Zoulalian, A., Celzard, A., 2009. Activated carbons prepared from wood particleboard wastes: characterisation and phenol adsorption capacities. J. Hazard Mater. 166 (1), 491–501.

Goher, M.E., Hassan, A.M., Abdel-Moniem, I.A., Fahmy, A.H., Abdo, M.H., El-sayed, S.M., 2015. Removal of aluminum, iron and manganese ions from industrial wastes using granular activated carbon and Amberlite IR-120H. Egypt. J. Aquat. Res. 41 (2), 155–164.

Gorzin, F., Bahri Rasht Abadi, M.M., 2018. Adsorption of Cr (VI) from aqueous solution by adsorbent prepared from paper mill sludge: kinetics and thermodynamics studies. Adsorpt. Sci. Technol. 36 (1–2), 149–169.

Hameed, B.H., 2009. Evaluation of papaya seeds as a novel non-conventional low-cost adsorbent for removal of methylene blue. J. Hazard Mater. 162 (2–3), 939–944.

Harvey Jr., A.E., Smart, J.A., Amis, E.S., 1955. Simultaneous spectrophotometric determination of iron (II) and total iron with 1, 10-phenanthroline. Anal. Chem. 27 (1), 26–29.

Hove, M., van Hille, R.P., Lewis, A.E., 2007. Iron solids formed from oxidation precipitation of ferrous sulfate solutions. AIChE J. 53 (10), 2569–2577.

Indhumathi, P., Syed Shabudeen, P.S., Shoba, U.S., Saraswathy, C.P., 2014. The removal of chromium from aqueous solution by using green micro algae. J. Chem. Pharm. Res. 6 (6), 799–808.

Jusoh, A., Cheng, W.H., Low, W.M., Nora'aini, A., Noor, M.M.M., 2005. Study on the removal of iron and manganese in groundwater by granular activated carbon. Desalination 182 (1–3), 347–353.

Kadirvelu, K., Kavipriya, M., Karthika, C., Radhika, M., Vennilamani, N., Pattabhi, S., 2003. Utilization of various agricultural wastes for activated carbon preparation and application for the removal of dyes and metal ions from aqueous solutions. Bioresour. Technol. 87 (1), 129–132.

Kadirvelu, K., Senthilkumar, P., Thamaraiselvi, K., Subburam, V., 2002. Activated carbon prepared from biomass as adsorbent: elimination of Ni (II) from aqueous solution. Bioresour. Technol. 81 (1), 87–90.

Kadirvelu, K., Thamaraiselvi, K., Namasivayam, C., 2001. Removal of heavy metals from industrial wastewaters by adsorption onto activated carbon prepared from an agricultural solid waste. Bioresour. Technol. 76 (1), 63–65.

Kavitha, D., Namasivayam, C., 2008. Capacity of activated carbon in the removal of acid brilliant blue: determination of equilibrium and kinetic model parameters. Chem. Eng. J. 139 (3), 453–461.

Kołodyńska, D., Krukowska, J.A., Thomas, P., 2017. Comparison of sorption and desorption studies of heavy metal ions from biochar and commercial active carbon. Chem. Eng. J. 307, 353–363.

Kundu, S., Gupta, A.K., 2006. Arsenic adsorption onto iron oxide-coated cement (IOCC): regression analysis of equilibrium data with several isotherm models and their optimization. Chem. Eng. J. 122 (1–2), 93–106.

Liew, R.K., Chai, C., Yek, P.N.Y., Phang, X.Y., Chong, M.Y., Nam, W.L., et al., 2019. Innovative production of highly porous carbon for industrial effluent remediation via microwave vacuum pyrolysis plus sodium-potassium hydroxide mixture activation. J. Clean. Prod. 208, 1436–1445.

Lazaroff, N., Sigal, W., Wasserman, A., 1982. Iron oxidation and precipitation of ferric hydroxysulfates by resting Thiobacillus ferrooxidans cells. Appl. Environ. Microbiol. 43 (4), 924–938.

Liang, S., Guo, X., Feng, N., Tian, Q., 2010. Isotherms, kinetics and thermodynamic studies of adsorption of Cu2+ from aqueous solutions by Mg2+/K+ type orange peel adsorbents. J. Hazard Mater. 174 (1–3), 756–762.

Majzlan, J., Myneni, S.C., 2005. Speciation of iron and sulfate in acid waters: aqueous clusters to mineral precipitates. Environ. Sci. Technol. 39 (1), 188–194.

Peng, W., Liu, Y.J., Wu, N., Sun, T., He, X.Y., Gao, Y.X., Wu, C.J., 2015. Areca catechu L. (Arecaceae): a review of its traditional uses, botany, phytochemistry, pharmacology and toxicology. J. Ethnopharmacol. 164, 340–356.

Rahman, M., Adil, M., Yusof, A., Kamaruzzaman, Y., Ansary, R., 2014. Removal of heavy metal ions with acid activated carbons derived from oil palm and coconut shells. Materials 7 (5), 3634–3650.

Selvaraju, G., Bakar, N.K.A., 2017. Production of a new industrially viable green-activated carbon from Artocarpus integer fruit processing waste and evaluation of its chemical, morphological and adsorption properties. J. Clean. Prod. 141, 989–999.

Supriadi, C.P., Kartini, E., Honggowiranto, W., Tri, K., 2017. Synthesis and characterization of carbon material obtained from coconut coir dust by hydrothermal and pyrolytic processes. Int. J. Technol. 2017 (8), 1470–1478.

Wu, F.C., Tseng, R.L., Juang, R.S., 2009. Initial behavior of intraparticle diffusion model used in the description of adsorption kinetics. Chem. Eng. J. 153 (1–3), 1–8.